Journal of Sustainable Development of Energy, Water and Environment Systems

http://www.sdewes.org/jsdewes

Year 2025, Volume 13, Issue 4, 1130613

Original Research Article

Enhanced Spectral Analysis Approaches for Predicting Critical Failures in Lithium-Ion Batteries: A Wavelet-Based Framework

Mario Carbonó de la Rosa[1], Jazael Gómez[2], Adalberto Ospino-Castro[*3], José Miguel Sánchez-De-La-Hoz[3], Carlos Robles-Algarín[4]

[1]Escuela de Ciencias Básicas Ingeniería y Tecnología, Universidad Nacional Abierta y a Distancia, Calle 14 Sur # 14 – 23, Bogotá, Colombia
e-mail: mario.carbono@unad.edu.co

[2]Instituto de Energías Renovables, Universidad Nacional Autónoma de México, Privada Xochicalco S/N, 62580 Temixco, México
e-mail: jagoo@ier.unam.mx

[3]Programa de Ingeniería Eléctrica, Universidad de la Costa, Calle 58 No. 55 – 66, Barranquilla, Colombia
e-mail: aospino8@cuc.edu.co; jsanchez80@cuc.edu.co

[4]Facultad de Ingeniería, Universidad del Magdalena, Carrera 32 No. 22-08, Santa Marta, Colombia
e-mail: croblesa@unimagdalena.edu.co

Cite as: Carbono dela Rosa, M. E., Gómez, J., Ospino, A., Sánchez-De-La-Hoz, J. M., Robles, C., Enhanced Spectral Analysis Approaches for Predicting Critical Failures in Lithium-Ion Batteries: A Wavelet-Based Framework, J.sustain. dev. energy water environ. syst., 13(4), 1130613, 2025, DOI: https://doi.org/10.13044/j.sdewes.d13.0613

ABSTRACT

This study presents an enhanced spectral framework for early fault detection in lithium-ion batteries, focused on analysing voltage and current fluctuations in silicon–carbon half-cells. The method integrates fast Fourier transform, continuous wavelet transform, cross-wavelet transform, and wavelet transform coherence to extract time–frequency features associated with degradation. Results reveal the emergence of low-frequency spectral modulations and phase coherence losses that precede critical failure events. The approach was validated across three independent silicon–carbon cells, demonstrating high reproducibility of fault indicators. Given its low computational footprint and diagnostic accuracy, the proposed method shows strong potential for implementation in battery management systems for predictive maintenance and real-time health monitoring.

KEYWORDS

Lithium-ion battery, Early fault-detection, Wavelet transform, Spectral analysis, Predictive maintenance, Half-cells.

INTRODUCTION

The global transition to cleaner energy sources has intensified research efforts in energy storage technologies, particularly lithium-ion batteries, due to their superior energy density and efficiency [1]. With the rising adoption of electric vehicles (EVs), hybrid electric vehicles (HEVs), and grid-scale storage solutions, ensuring battery safety has become paramount. Despite their advantages, lithium-ion batteries present significant safety concerns, as failures such as overheating, over-discharge, and internal short circuits can lead to catastrophic outcomes [2]. Addressing these challenges requires advanced diagnostic techniques capable of detecting early signs of failure [3].

* Corresponding author

Although electric vehicles (EVs) have existed for more than a century, their large-scale integration has accelerated only in recent decades due to advances in lithium-ion battery technology, improved energy density, and stricter environmental regulations. This evolution underscores the critical importance of ensuring battery safety and reliability under dynamic usage conditions, where early fault detection becomes essential [4].

Today, electric vehicles (EVs) have re-emerged as a viable solution to environmental challenges, primarily due to their energy efficiency and zero-emission performance. Unlike internal combustion engine vehicles, EVs do not emit harmful pollutants such as carbon dioxide, sulphur oxides, nitrogen oxides, or particulate matter, making them a cleaner alternative for urban mobility [5]. Furthermore, their electric motors demonstrate superior efficiency, converting a larger proportion of electrical energy into mechanical motion across a wide range of speeds, thereby eliminating the need for complex gearboxes or transmission systems [6]. This simplicity in drivetrain design not only enhances efficiency but also improves reliability and maintenance [7]. Additionally, the near-silent operation of EVs helps reduce noise pollution in densely populated areas, providing a more comfortable and quieter urban environment [8].

Significant progress in materials science and electronics over the past few decades has facilitated the revival of battery technology, initially with nickel-metal hydride (NiMH) and later with lithium-ion (Li-ion) cells. These advancements have been crucial in accelerating the large-scale adoption of electric vehicles, primarily by improving energy storage efficiency and operational safety [9]. Historical data indicate that the energy density of Li-ion batteries has increased 2.5-fold since 2008, while production costs have dropped by approximately 81% [10]. However, these advancements come with notable safety challenges. The increased energy density and faster charging capabilities have introduced risks related to thermal instability, making early fault detection a critical yet unresolved issue. Malfunctions such as overheating and excessive discharge can escalate into severe failures if not identified promptly [11].

Recent studies have explored various aspects of battery management and electric vehicle integration to address these challenges. A multi-criteria decision-making model to assist EV users in selecting optimal charging stations—considering factors such as charging cost, waiting time, and energy source sustainability—was developed in [12], thereby enhancing charging efficiency and user satisfaction. The relationship between the state of health of batteries with liquid electrolytes and changes in transmittance at specific frequencies was investigated in [13], offering a novel, non-destructive method for assessing battery degradation. A comprehensive numerical thermal model of a lithium iron phosphate (LFP) battery pack for residential applications was presented in [14], providing insights into thermal behaviour under various operating conditions, which is crucial for safety and efficiency. A simple photovoltaic electric vehicle charging management system that considers sun availability time to reduce carbon emissions was proposed in [15], supporting the integration of renewable sources into EV charging infrastructure. Finally, a method to model the hourly variability of renewable energy sources in integrated assessment models was introduced in [16], bridging operational and long-term planning needs in decarbonisation scenarios.

Building on these developments, fault diagnosis techniques for lithium-ion batteries have been significantly enhanced through the integration of time–frequency analysis and hybrid signal processing methods. A wavelet packet decomposition approach for identifying faults in EV power batteries was introduced in [17], demonstrating superior accuracy compared to traditional Fourier-based techniques. A voltage fault detection strategy using continuous wavelet transform and image entropy was developed in [18], effectively capturing transient anomalies in high-resolution battery signals. A comprehensive comparison of nonlinear estimation algorithms—including Extended Kalman Filter, Unscented Kalman Filter, and Particle Filter—for online SoC and SoH prediction in lithium-ion batteries was presented in [19], revealing trade-offs between computational complexity and predictive accuracy under dynamic load conditions. In [20], a diagnostic method based on half-cell electrode potentials

achieved a maximum state-of-health estimation error of 1.44%, while a recent review in [21] outlined observer-based and model-driven techniques for improving early-stage battery fault detection under variable operating scenarios.

Unlike the previous study conducted by the authors, which focused solely on spectral analysis of voltage signals using the Fourier and continuous wavelet transform (CWT), the current research introduces a hybrid framework incorporating cross-wavelet transform (XWT) and wavelet transform coherence (WTC) between voltage and current signals. This dual-signal analysis provides insight into the time–frequency correlation structure between electrical variables, enabling more sensitive detection of fault-related spectral coupling. The application of XWT and WTC allows for identification of both phase and coherence anomalies, which are not accessible through single-signal analysis techniques. To our knowledge, this is the first study to apply this integrated spectral framework to Si–C half-cell degradation signals for predictive diagnostics.

Incidents such as spontaneous battery fires in electric vehicles, along with high-profile cases such as the Boeing 787 failure, have impeded widespread adoption and led to significant financial losses for manufacturers. The Boeing investigation highlighted the challenges in identifying the root causes of lithium-ion battery malfunctions and underscored the need for more rigorous qualification procedures and safety assessment methodologies [22]. One of the main contributors to such failures is the limited capability of current battery management systems (BMS) to accurately predict and mitigate critical faults—such as overheating, over-discharge, or internal short circuits—in real time. Recent research has proposed on-line life-cycle health assessment methods that rely on measurable electrical parameters to monitor degradation and improve capacity estimation under dynamic conditions [23]. In parallel, effective thermal regulation remains essential; studies comparing nanofluid-based submerged and circulated cooling strategies have demonstrated their potential to maintain operational safety and enhance the reliability of battery systems across varying environmental and discharge conditions [24].

This study presents a novel hybrid spectral analysis approach that integrates Fourier and wavelet transformations to detect early-stage degradation in lithium-ion batteries (LIBs). Cycling data from silicon–carbon anode half-cells are analysed, leveraging spectral decomposition to identify characteristic frequency shifts associated with failure modes. The results highlight the feasibility of this approach for real-time monitoring and predictive maintenance in energy storage applications.

MATERIALS AND METHODS

This study proposes a multi-stage time-frequency analysis to extract failure-related features from lithium-ion battery cycling tests. In this context, the computational study focuses on half-cell configurations with silicon-carbon anodes, which represent a promising alternative for high-capacity energy storage. The experimental protocol follows standardised charge/discharge cycles while capturing voltage and current variations for subsequent spectral analysis.

Figure 1 presents the workflow, which consists of four main phases: (i) data acquisition from controlled cycling experiments, (ii) signal preprocessing and noise filtering, (iii) spectral decomposition via Fourier and wavelet transforms, and (iv) fault detection based on characteristic frequency anomalies. To ensure robust feature extraction, the Morlet wavelet is employed, offering high temporal and frequency resolution—essential for identifying early-stage battery degradation. Its proven effectiveness in analysing transient and oscillatory behaviour in non-stationary signals makes it particularly suitable for this application. This wavelet, composed of a complex sinusoid modulated by a Gaussian envelope, offers an optimal balance between time and frequency resolution, making it suitable for identifying subtle variations in battery voltage and current profiles. Compared to other wavelet families such as Daubechies or Mexican Hat, the Morlet wavelet maintains better frequency localization while preserving acceptable time

sensitivity, which is essential for isolating low-frequency degradation patterns and short-lived anomalies. Previous studies have demonstrated the reliability of discrete wavelet transform-based methods for feature extraction and fault detection in lithium-ion batteries [25]. Additionally, novel wavelet-based approaches have proven effective in assessing cell-to-cell consistency through experimental voltage signal analysis [26].

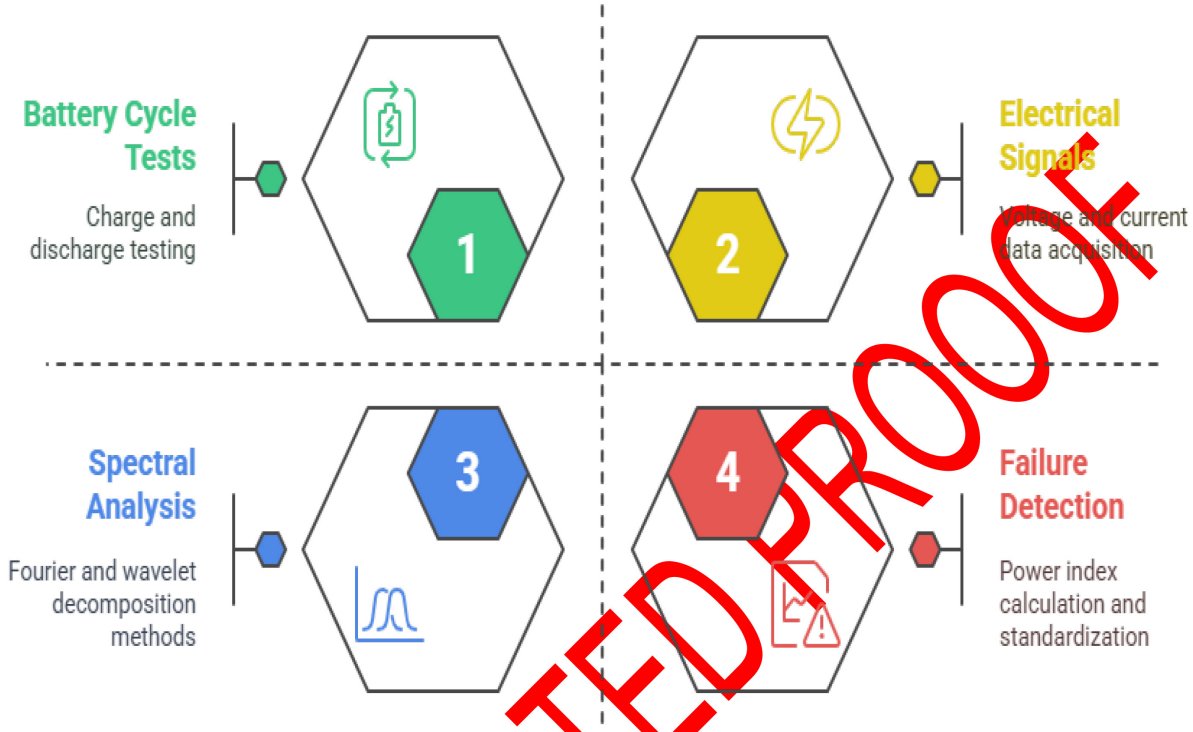

Figure 1. Workflow of the proposed time-frequency analytical approach for the early detection of battery failures

The analysis of cycling test data was performed on SXC cells (Silicon Experimental Cells), specifically SXC-1, SXC-2, and SXC-3, which utilized silicon mesh as the working electrode and a lithium metal counter electrode. These evaluations followed a structured charge/discharge framework (refer to Table 1), where the charging phase was conducted under a direct current (DC) protocol, ensuring a steady flow until the designated cut-off voltage was attained. The cycling experiments were carried out using an 8-channel battery analyser (Model BST8-MA, 10 mA precision, MTI Corporation, USA), powered at 110 VAC ±10% and rated for 30 W. This system allows for individual control and logging of each cell with high current resolution and stable voltage acquisition. The measurements were acquired at a 1 Hz sampling rate, ensuring adequate temporal resolution to capture dynamic behaviours across full cycling profiles.

Table 1. Specifications of the evaluated lithium-ion cell (CC: Constant current, CV: constant voltage)

	Charge		Discharge			
Cell	CC [mA/g]	Cut off voltage [V]	CC [mA/g]	CV [V]	Cycles	T [°C]
SXC-1	100	1.3	100	0.1	100	25
SXC-2	100	1.3	100	0.1	74	25
SXC-3	100	1.3	100	0.1	42	25

A corresponding discharge cycle was executed in an identical manner to complete the charge/discharge process. The cycle was systematically repeated multiple times to generate consistent and reliable experimental data. The SXC cells were designed for the experimental validation of silicon-carbon anode performance, offering high theoretical capacity and potential improvements in energy storage efficiency. The summarised findings from these tests are provided in Table 2.

Table 2. Performance parameters of the evaluated lithium-ion cell

Cell type	Cathode	Anode	Capacity [mAh/g]
Half-cell	Si/C	Li	300

RESULTS AND DISCUSSION

The spectral analysis of half-cell voltage cycling data reveals distinct frequency patterns preceding failure events. Fourier spectra demonstrate that, while the primary cycling frequency remains stable, additional harmonics emerge prior to critical degradation. Continuous wavelet transform (CWT) analysis further illustrates transient frequency shifts associated with capacity loss and abnormal electrochemical behaviour.

A range of MATLAB-based resources, including the Wavelet Toolbox, signal processing libraries, and specialised FFT and WT functions, were employed for data transformation. In accordance with the Nyquist-Shannon sampling theorem [27], the sampling frequency (SF) for FFT calculations was set to at least twice the maximum frequency detected in the voltage cycle. This configuration was crucial in ensuring precise spectral representation, minimising aliasing, and preserving signal accuracy throughout the analysis.

Cross-wavelet transform (XWT) analysis of voltage and current signals indicates phase synchronisation disruptions prior to failure. Coherence wavelet transform (WTC) results suggest that frequency bands associated with degradation exhibit decreasing coherence, highlighting the progressive loss of charge retention capability.

Frequency spectrum of cycling voltage

To highlight the primary frequency components and identify those associated with abnormalities or potential malfunctions in the batteries, the Fourier spectrum range was refined. Figure 2d illustrates the voltage signal spectrum of the SXC-1 battery, evaluated by IER-UNAM under controlled conditions at 25°C, while additional spectra for SXC-2 and SXC-3 are provided in Figure S1d and Figure S2d within the supplementary materials.

Across the three cycling tests, the charge-discharge voltage cycle remained stable, with the dominant frequency measured at 0.509 Hz, corresponding to a 1.96-hour cycle. Minor frequency components, particularly those below 4.24×10^{-2} Hz, are difficult to distinguish in Figure 2d. An inconsistent spectral pattern is observed in the 0.58–1.56 Hz range; however, no direct correlation with battery degradation or failure has been established.

Time – frequency analysis by the continuous wavelet transforms

The evaluation of battery voltage signals over time, obtained from half-cell (SXC-1) cycling experiments, was transformed into the time-frequency domain using the continuous wavelet transform (CWT). This transformation was performed through a set of wavelets generated via dilation and shifting of the mother wavelet.

For this study, the Morlet wavelet was selected as the mother wavelet due to its effectiveness in capturing localized spectral power variations across different periodic scales. This choice enabled an in-depth examination of power fluctuations within the non-stationary time series of battery voltage, which contains multiple cyclic patterns [28]. The Morlet wavelet provides high resolution across frequency scales and being a complex wavelet, facilitates signal filtering into

specific bandwidths [29]. The colour scale on the right side of Figure 2b, Figure 3b and Figure 4b represents spectral power distribution, where deep red indicates the highest power intensity and blue the lowest.

In Figure 2c, the time-frequency representation of the SXC-1 battery voltage, obtained from IER-UNAM tests, is illustrated using CWT. A distinct deep red section in the mid-region of the wavelet spectrum highlights a principal periodicity of approximately 2 hours, aligning with the global wavelet results (Figure 2b). Disturbances in the cycling pattern distort this spectral region, altering its shape. Around the 30-hour mark, a shift in the charge rate (C-rate) of the voltage signal becomes evident, introducing frequency variations that contribute to spectral anomalies. Additionally, a horizontally extended area of lower spectral intensity, characterized by light green shades, emerges beneath the primary waveform and expands as the voltage cycle is modified.

An analysis of the dataset reveals that, at this specific moment, the battery's capacity exhibited a noticeable decline, suggesting that these periodic variations may be associated with a brief internal fault affecting performance. Comparable anomalies appear in the wavelet spectral power at the 47-hour mark, coinciding with an additional capacity reduction, although such inconsistencies are barely discernible in the voltage time series. Beyond 50 hours, the wavelet spectrum shows a gradual decline in primary periodicity relative to the time scale, indicating an increase in the C-rate of voltage cycling, as depicted in Figure 2a. This trend suggests a progressive degradation in the battery's ability to store energy efficiently.

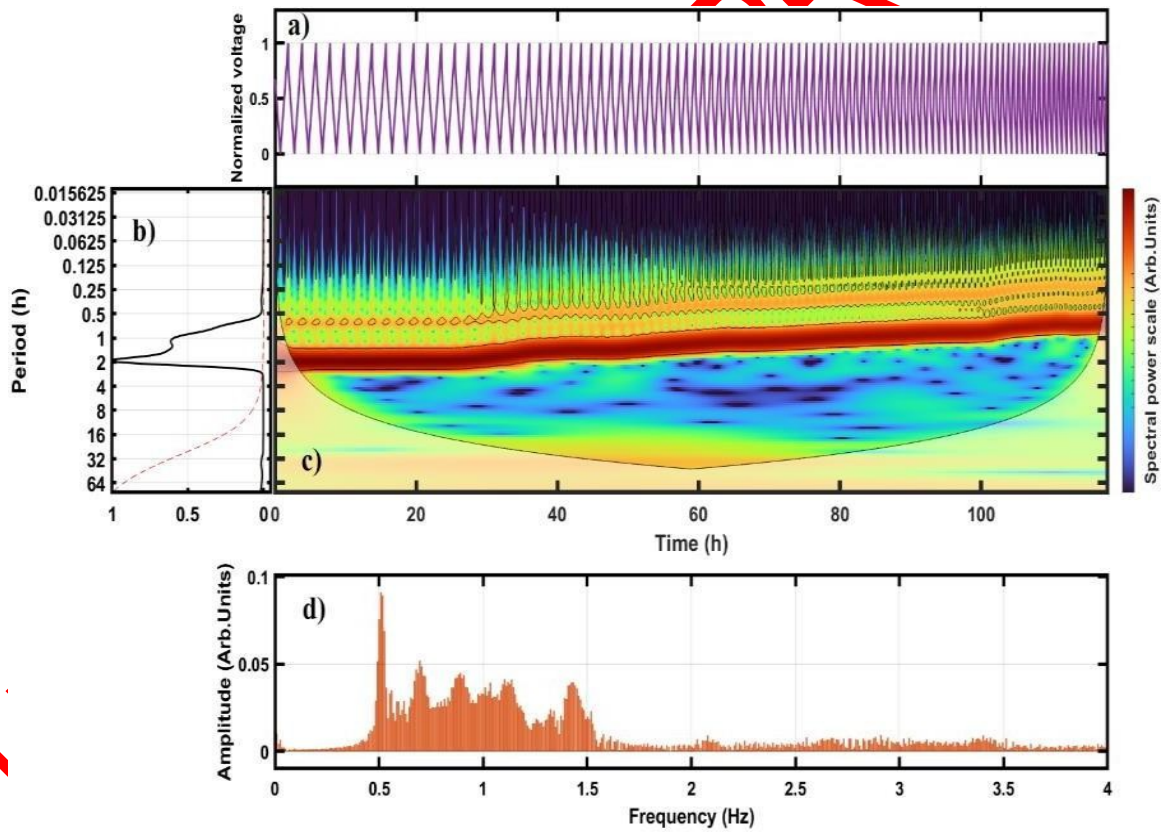

Figure 2. Time-frequency analysis of the SXC-1 battery voltage using CWT and Fourier Transform: (a) Battery voltage time series; (b) Global wavelet spectrum (black curve) with the 95% red-noise confidence threshold (red dashed line); (c) Time-frequency representation obtained via CWT, where the black curve marks the COI; and (d) Fourier spectrum analysis of the cycling experiment

As observed in the global wavelet representation, shortly before reaching 100 hours, a set of higher-frequency components emerges above the primary periodicity, centred at approximately 1 hour. These high-energy spectral intervals coincide with the second most prominent amplitude peak identified in the non-uniform spectrum shown in Figure 2d. Database records indicate that

before these frequency variations appeared, the battery had already experienced a capacity loss exceeding 55%. Figure S1c and Figure S2c in the supplementary materials illustrate the wavelet spectral power for SXC-2 and SXC-3 cells, neither of which exhibited signs of critical failure during testing.

Time frequency analysis using the cross wavelet transform

Hudgins et al. [30] developed the cross-wavelet spectrum as a technique to analyse the interdependent behaviour of two variables, X and Y. This method assesses their phase and frequency synchronisation, providing insight into their dynamic correlation [31]. The cross-wavelet function (WXY) is defined by Eq. 1, as follows:

$$W_{xy} = W_x \circledast W_y^* \tag{1}$$

In this context, $\circledast$ represents the Hadamard product, while (*) denotes the complex conjugation operation. The symbols Wx and Wy correspond to the wavelet transforms of two time series, X and Y, which represent the normalised voltage and current intensity measurements obtained from the SXC-1 battery cycling test, as illustrated in Figure 3a. Additionally, Figure 3c presents the cross-wavelet transform (XWT) results, depicting the interrelation between both time series through the wavelet power spectrum. The directional arrows in this figure indicate the phase relationship between voltage and current across the time–frequency domain. Specifically, arrows pointing directly to the right ($\rightarrow 0^\circ$) or left ($\leftarrow 180^\circ$) indicate linear synchronisation, implying an in-phase or anti-phase association between the two variables at a given frequency. Deviations from these alignments suggest a more complex, nonlinear synchronisation pattern [32].

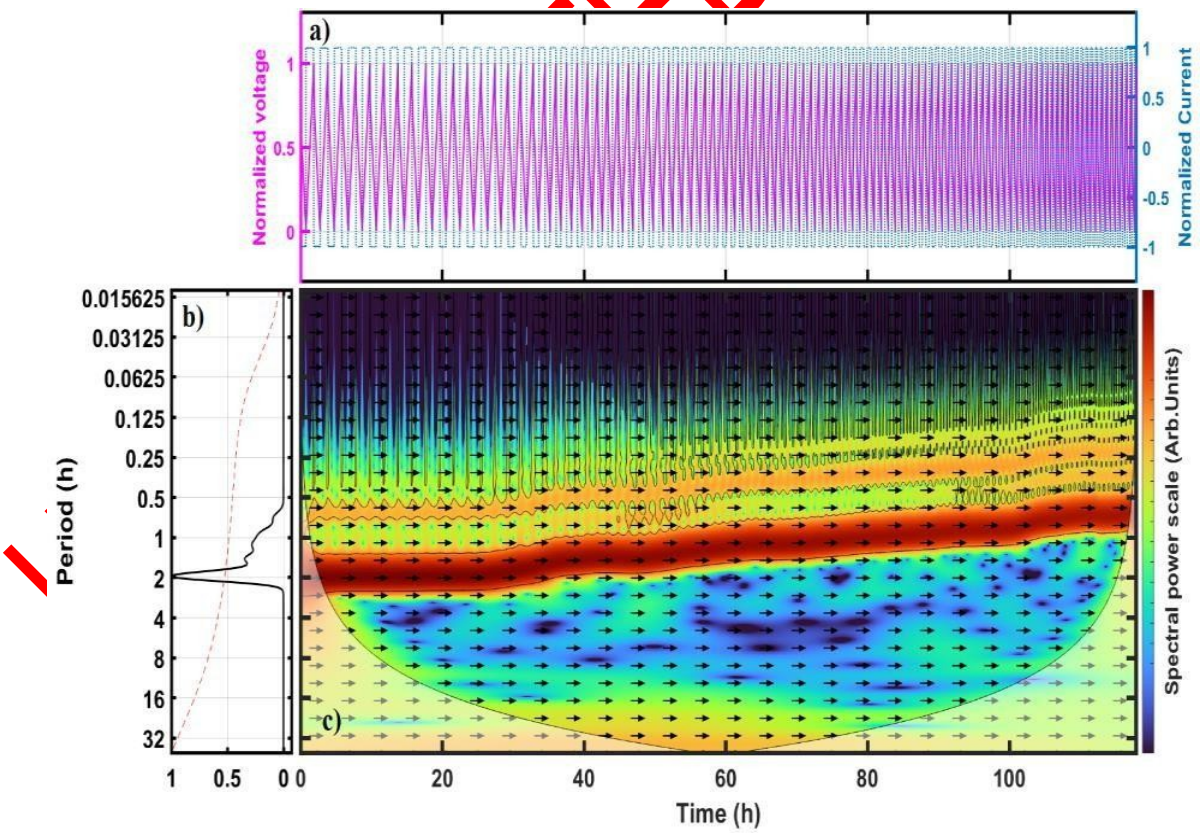

Figure 3. Time-frequency analysis of the cycling test for the SXC-1 cell using XWT: (a) Time series of current and battery voltage; (b) Global wavelet spectrum (black curve) with the 95% red-noise confidence threshold (red dashed line); and (c) XWT spectral power, where the curved black line marks the COI

This analysis demonstrates that the two signals exhibit phase coherence over the studied time and frequency ranges. Furthermore, Figure 3b of the global wavelet spectrum reveals additional periodicities at frequencies lower than the primary one. Complementary findings are available in the supplementary material, where Figure S3c and Figure S4c illustrate the XWT spectral power for the SXC-2 and SXC-3 cells, both of which remained free from critical failure throughout the evaluation.

Time – frequency analysis using wavelet transforms coherence

Wavelet transform coherence (WTC) was obtained by applying a smoothing process to both the temporal and frequency scales of the cross-wavelet spectrum. Its purpose is to identify specific frequency ranges and time segments where the analysed time series exhibit a relationship [33]. This approach enables the evaluation of localised correlation coefficients and phase interactions between two time series that display non-stationary power fluctuations across multiple frequencies [34]. The WTC in [35] is defined as:

$$R_{xy}(\tau, s) = \frac{\left|S\left(W_{xy}(\tau, s)\right)\right|}{S(|W_x(\tau, s)|^2)S\left(\left|W_y(\tau, s)\right|^2\right)} \quad (2)$$

R_{xy} takes values between 0 and 1, while S is a smoothing operator applied to both time and frequency (without S, the wavelet coherence would always be equal to 1 at all scales). Values closer to one indicate a stronger correlation, whereas values approaching 0 suggest a weaker relationship [36]. Figure 4a shows the two-time series in normalised units that were analysed with the WTC: the first corresponds to the voltage signal (magenta solid line), while the second represents the battery charge/discharge current (blue dashed line).

Figure 4c presents the coherence analysis results, illustrating the correlation between battery voltage and current by assessing the local covariance of these two-time series across different time and frequency scales. The global wavelet spectrum highlights a region of maximum spectral power density occurring between 4 and 0.05 hours, depicted in dark red. Within this zone, a frequency range spanning 3.5 to 1.5 hours is associated with the primary cycling periodicities (refer to Figure 4b and Figure 4c). Similar to the observations in Figure 3c and Figure 2c, the main periodicity exhibits interruptions and a declining trend due to progressive capacity loss. Additionally, periodic components near 1 hour emerge sporadically between 0–46 hours and 56–87 hours, displaying irregular spectral power at moderate-to-low intensity.

Within the XWT analysis, the direction of the arrows and their corresponding phase angles illustrate the degree of correlation between two time series at varying scales. Arrows oriented vertically—either upward or downward—correspond to phase shifts of π/2 and -π/2, respectively, indicating that one variable precedes or lags the other. Alternatively, when an arrow points to the right with a phase angle ϕ_{xy} in the range (0, π/2) or (-π, -π/2), it suggests that the second variable leads the first. Conversely, if ϕ_{xy} falls between (-π/2, 0) or (π/2, π), the first variable leads the second [37].

Figure 4c shows the wavelet transform coherence (WTC) map, quantifying the localized correlation between voltage and current signals across time and frequency scales. The high-power regions in dark red (4 to 0.05 hours) indicate strong phase coupling during regular cycling activity. Within this zone, dominant periodicities between 3.5 and 1.5 hours align with the core cycling frequencies identified in Figure 4b. Early in the test (0–100 hours), most phase arrows point to the right at angles near π/4, implying that current variations precede voltage responses—a behaviour consistent with expected electrochemical dynamics. After 100 hours, the phase angle progressively approaches zero, denoting increasing synchrony between the two signals. This transition may be linked to capacity fading or aging-induced impedance shifts.

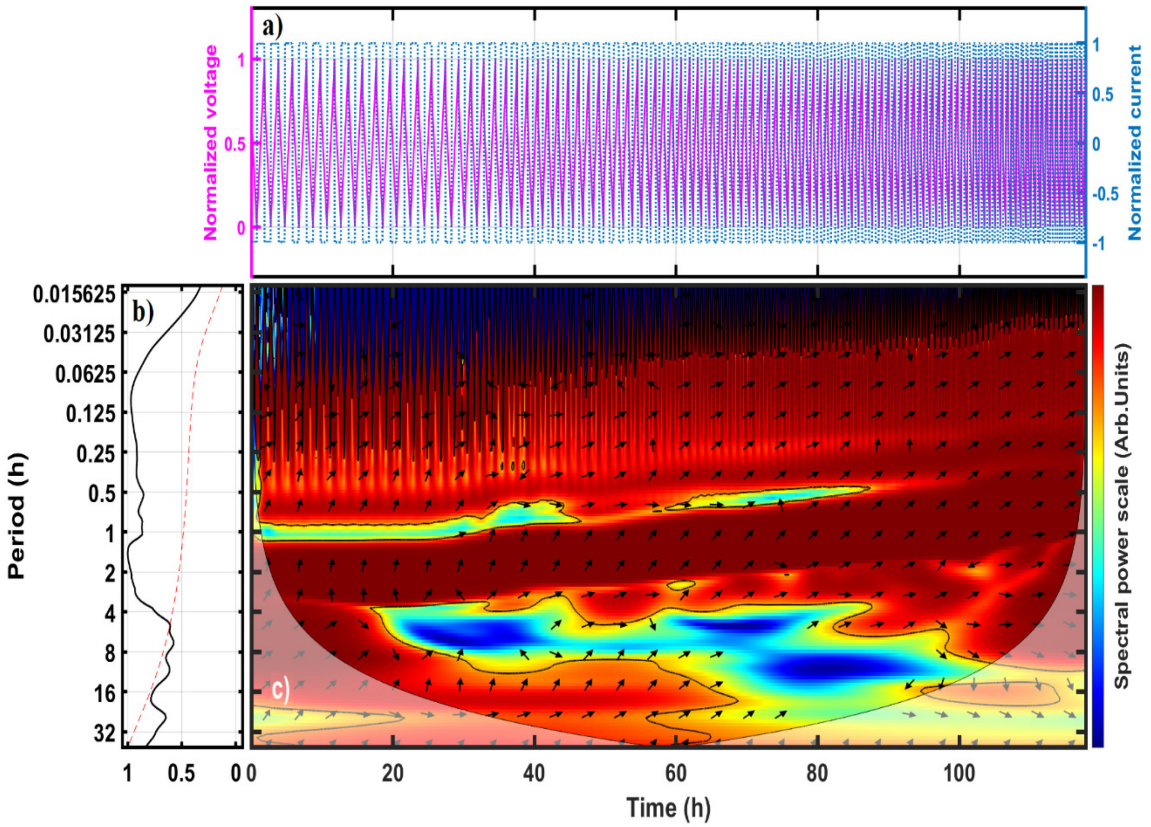

Figure 4. Time-frequency analysis of the cycling test for the SXC-1 cell using WTC: (a) Time series of current and battery voltage; (b) Global wavelet spectrum (black curve) with the 95% red-noise confidence threshold (red dashed line); and (c) WTC spectral power, where the curved black line marks the COI

Supplementary Figure S5c and Figure S6c, corresponding to SXC-2 and SXC-3, reveal similar spectral coherence structures, with no indication of abrupt failures. However, a steady phase offset near $\pi/2$ remains visible in the dominant frequency band, further confirming that current leads voltage even in non-failing cells. The evolution of phase synchronization and coherence loss supports the use of WTC as a diagnostic indicator of electrochemical degradation.

A comparative analysis was performed across the three half-cells (SXC-1, SXC-2, and SXC-3) to evaluate the repeatability of the spectral patterns identified. The supplementary figures corresponding to each transform (Figure S1–S6) demonstrate that SXC-2 and SXC-3 reproduce the key spectral signatures observed in SXC-1. In the FFT domain (Figure 2), all three cells exhibit a progressive energy concentration in the low-frequency range as cycling advances, indicating consistent degradation behaviour. The CWT analysis (Figure S1 and Figure S2) revealed time-localized anomalies near the end of life for each cell, with the Morlet-based transform capturing envelope fluctuations and transient events at comparable scales. XWT plots (Figure S3 and Figure S4) confirm the presence of phase-locked frequency components during late-stage cycles, consistent with the degradation-induced coupling observed in SXC-1. Moreover, the WTC maps (Figure S5 and Figure S6) show coherence decay and shifts in phase alignment in the 0.002–0.008 Hz range, particularly during cycles beyond 200, reinforcing the interpretation of fault progression. These consistencies validate the robustness of the proposed hybrid spectral approach for early fault detection in Si–C half-cells under dynamic load conditions.

CONCLUSIONS

A spectral analysis was performed on the charge/discharge test cycle voltage of lithium-ion batteries with a silicon-carbon anode. The Fourier transform was employed to identify the primary

frequencies of the cycles and the harmonic components present in the voltage signal. A complementary analysis using continuous, cross, and coherence wavelet transforms revealed significant patterns in the battery cycling tests.

Firstly, prior to an irregular event, critical failure, or battery degradation, the continuous and cross wavelet transform figures exhibit the emergence of new frequency components following a change in the main periodicity of the voltage signal. Secondly, the coherence wavelet transform reveals discontinuous periodicity intervals with medium-to-low spectral power, a time lag between the time series where the current precedes the voltage, and a declining trend in the main periodicity associated with a loss of battery capacity.

This study reinforces the potential of spectral analysis for early fault detection in lithium-ion batteries. The findings demonstrate that frequency-domain features extracted via Fourier and wavelet transformations provide valuable insights into battery health. The emergence of new frequency components serves as an early warning indicator of impending failures, offering a predictive framework for battery management systems (BMS) to detect early signs of degradation, capacity loss, and failure. This approach can significantly reduce the risk of critical failures in electric vehicle battery systems. Beyond applications in electric vehicle batteries, the proposed spectral analysis methodology could be extended to other energy storage technologies where early fault detection is crucial. By enhancing the safety and reliability of these systems, this method supports the broader adoption of energy storage in renewable energy grids, where the stability and longevity of storage solutions are paramount.

Future research should explore the scalability of this methodology across different battery chemistries, including solid-state and sodium-ion technologies. Finally, the proposed framework could be adapted to other lithium-based chemistries, provided that their spectral response characteristics are well characterized. Furthermore, the method shows potential for integration into real-time battery management systems (BMS), particularly in scenarios where signal distortions serve as early indicators of degradation. While the approach is computationally efficient, practical deployment would require addressing several key challenges, including ensuring an adequate data acquisition rate (typically >1 Hz) to resolve transient features, optimizing processing resources for real-time execution, and ensuring sensor accuracy to minimize signal noise. These considerations will guide future work focused on embedded implementation and testing under dynamic load conditions.

ACKNOWLEDGMENTS

The authors would like to acknowledge to Universidad Nacional Abierta y a Distancia de Colombia, Universidad Nacional Autónoma de México, Universidad de la Costa, Universidad del Magdalena and Prenteck Ingeniería for their support in the development of this research.

NOMENCLATURE

CC	Constant Current (charge/discharge current)	[mA/g]
CV	Constant Voltage	[V]
T	Temperature	[°C]
W_x	Wavelet transform of time series X (e.g. voltage signal)	–
W_y	Wavelet transform of time series Y (e.g. current signal)	–
$\circledast$	Hadamard product operator	–
*	Complex conjugation operator	–
R_{xy}	Wavelet coherence coefficient between time series X and Y	–

S	Smoothing operator (applied to time and frequency scales in WTC) –

Abbreviations

EVs	Electric Vehicles
HEVs	Hybrid Electric Vehicles
CWT	Continuous Wavelet Transform
SF	Sampling Frequency
COI	Cone of Influence (limit for reliable period detection in the time–frequency domain)
C-rate	Charge rate (indicator of battery charging/discharging intensity)
XWT	Cross-Wavelet Transform
WTC	Wavelet Transform Coherence
FFT	Fast Fourier Transform
BMS	Battery Management System
LIBs	Lithium-Ion Batteries
SXC	Silicon Experimental Cell
DC	Direct Current

REFERENCES

1. J. B. Goodenough and K.-S. Park, "The Li-Ion Rechargeable Battery: A Perspective," *J Am Chem Soc*, vol. 135, no. 4, pp. 1167–1176, Jan. 2013, https://doi.org/10.1021/ja3091438.
2. M. Armand and J.-M. Tarascon, "Building better batteries," *Nature*, vol. 451, no. 7179, pp. 652–657, Feb. 2008, https://doi.org/10.1038/451652a.
3. B. Dunn, H. Kamath, and J.-M. Tarascon, "Electrical Energy Storage for the Grid: A Battery of Choices," *Science (1979)*, vol. 334, no. 6058, pp. 928–935, Nov. 2011, https://doi.org/10.1126/science.1212741.
4. S. S. Zhang, "A review on electrolyte additives for lithium-ion batteries," *J Power Sources*, vol. 162, no. 2, pp. 1379–1394, Nov. 2006, https://doi.org/10.1016/j.jpowsour.2006.07.074.
5. P. G. Bruce, S. A. Freunberger, L. J. Hardwick, and J.-M. Tarascon, "Li–O2 and Li–S batteries with high energy storage," *Nat Mater*, vol. 11, no. 1, pp. 19–29, Jan. 2012, https://doi.org/10.1038/nmat3191.
6. M. S. Whittingham, "Lithium Batteries and Cathode Materials," *Chem Rev*, vol. 104, no. 10, pp. 4271–4302, Oct. 2004, https://doi.org/10.1021/cr020731c.
7. N. Nitta, F. Wu, J. T. Lee, and G. Yushin, "Li-ion battery materials: present and future," *Materials Today*, vol. 18, no. 5, pp. 252–264, Jun. 2015, https://doi.org/10.1016/j.mattod.2014.10.040.
8. F. Cheng, J. Liang, Z. Tao, and J. Chen, "Functional Materials for Rechargeable Batteries," *Advanced Materials*, vol. 23, no. 15, pp. 1695–1715, Apr. 2011, https://doi.org/10.1002/adma.201003587.
9. M.-C. Lin *et al.*, "An ultrafast rechargeable aluminium-ion battery," *Nature*, vol. 520, no. 7547, pp. 324–328, Apr. 2015, https://doi.org/10.1038/nature14340.
10. H.-J. Kim *et al.*, "A Comprehensive Review of Li-Ion Battery Materials and Their Recycling Techniques," *Electronics (Basel)*, vol. 9, no. 7, p. 1161, Jul. 2020, https://doi.org/10.3390/electronics9071161.

11. M. E. Carbonó dela Rosa *et al.*, "A New Methodology for Early Detection of Failures in Lithium-Ion Batteries," *Energies (Basel)*, vol. 16, no. 3, p. 1073, Jan. 2023, https://doi.org/10.3390/en16031073.
12. S. Karatzas, P. Farmakis, A. Chassiakos, T. Farmakis, Z. Christoforou, and G. Liappi, "Development of a multi criteria model for assisting EV user charging decisions," *Journal of Sustainable Development of Energy, Water and Environment Systems*, vol. 11, no. 2, pp. 1–23, Jun. 2023, https://doi.org/10.13044/j.sdewes.d10.0439.
13. J. A. Palacio, E. García, and W. Orozco, "State of health of liquid electrolyte batteries and its relationship with the change in transmittance at a frequency of 254nm," *Journal of Sustainable Development of Energy, Water and Environment Systems*, vol. 11, no. 4, pp. 1–11, Dec. 2023, https://doi.org/10.13044/j.sdewes.d11.0467.
14. M. Costa, A. Palombo, A. Ricci, and U. Sorge, "Thermal Behavior of a LFP Battery for Residential Applications: Development of a Multi-Physical Numerical Model," *Energy Engineering*, vol. 122, no. 5, pp. 1629–1643, 2025, https://doi.org/10.32604/ee.2025.062613.
15. S. Syafii, K. Krismadinata, M. Muladi, T. K. Agung, and D. Ananta Sandri, "Simple Photovoltaic Electric Vehicles Charging Management System Considering Sun Availability Time," *Journal of Sustainable Development of Energy, Water and Environment Systems*, vol. 12, no. 1, pp. 1–12, Mar. 2024, https://doi.org/10.13044/j.sdewes.d11.0476.
16. G. Parrado-Hernando, F. Frechoso-Escudero, and L. J. Miguel González, "Method to Model the Hourly Variability of Renewable Energy Sources in Integrated Assessment Models," *Journal of Sustainable Development of Energy, Water and Environment Systems*, vol. 12, no. 1, pp. 1–25, Mar. 2024, https://doi.org/10.13044/j.sdewes.d11.0481.
17. J. Jiang, R. Zhang, Y. Wu, C. Chang, and Y. Jiang, "A fault diagnosis method for electric vehicle power lithium battery based on wavelet packet decomposition," *J Energy Storage*, vol. 56, p. 105909, Dec. 2022, https://doi.org/10.1016/j.est.2022.105909.
18. C. Chang, Q. Wang, J. Jiang, Y. Jiang, and T. Wu, "Voltage fault diagnosis of a power battery based on wavelet time-frequency diagram," *Energy*, vol. 278, p. 127920, Sep. 2023, https://doi.org/10.1016/j.energy.2023.127920.
19. A. Papazoglou, S. Longo, D. Auger, and F. Assadian, "Nonlinear Filtering Techniques Comparison for Battery State Estimation," *Journal of Sustainable Development of Energy, Water and Environment Systems*, vol. 2, no. 3, pp. 259–269, Sep. 2014, https://doi.org/10.13044/j.sdewes.2014.02.0021.
20. C. Zhu, L. Sun, C. Chen, J. Tian, W. Shen, and R. Xiong, "Lithium-ion battery degradation diagnosis and state-of-health estimation with half cell electrode potential," *Electrochim Acta*, vol. 459, p. 142588, Aug. 2023, https://doi.org/10.1016/j.electacta.2023.142588.
21. Y. Zhou, Z. Ma, and L. Fu, "A Review of Key Signal Processing Techniques for Structural Health Monitoring: Highlighting Non-Parametric Time-Frequency Analysis, Adaptive Decomposition, and Deconvolution," *Algorithms*, vol. 18, no. 6, p. 318, May 2025, https://doi.org/10.3390/a18060318.
22. N. Williard, W. He, C. Hendricks, and M. Pecht, "Lessons Learned from the 787 Dreamliner Issue on Lithium-Ion Battery Reliability," *Energies (Basel)*, vol. 6, no. 9, pp. 4682–4695, Sep. 2013, https://doi.org/10.3390/en6094682.
23. D. Liu, Y. Song, L. Li, H. Liao, and Y. Peng, "On-line life cycle health assessment for lithium-ion battery in electric vehicles," *J Clean Prod*, vol. 199, pp. 1050–1065, Oct. 2018, https://doi.org/10.1016/j.jclepro.2018.06.182.
24. R. D. Jilte, R. Kumar, and M. H. Ahmadi, "Cooling performance of nanofluid submerged vs. nanofluid circulated battery thermal management systems," *J Clean Prod*, vol. 240, p. 118131, Dec. 2019, https://doi.org/10.1016/j.jclepro.2019.118131.

25. M. Zhang, W. Chen, J. Yin, and T. Feng, "Health Factor Extraction of Lithium-Ion Batteries Based on Discrete Wavelet Transform and SOH Prediction Based on CatBoost," *Energies (Basel)*, vol. 15, no. 15, p. 5331, Jul. 2022, https://doi.org/10.3390/en15155331.
26. J. Kim, "Discrete Wavelet Transform-Based Feature Extraction of Experimental Voltage Signal for Li-Ion Cell Consistency," *IEEE Trans Veh Technol*, vol. 65, no. 3, pp. 1150–1161, Mar. 2016, https://doi.org/10.1109/TVT.2015.2414936.
27. B. P. Lathi and R. A. Green, *Essentials of Digital Signal Processing*. Cambridge University Press, 2014.
28. C. Torrence and G. P. Compo, "A Practical Guide to Wavelet Analysis," *Bull Am Meteorol Soc*, vol. 79, no. 1, pp. 61–78, Jan. 1998, https://doi.org/10.1175/1520-0477(1998)079<0061:APGTWA>2.0.CO;2.
29. A. Grinsted, J. C. Moore, and S. Jevrejeva, "Application of the cross wavelet transform and wavelet coherence to geophysical time series," *Nonlinear Process Geophys*, vol. 11, no. 5/6, pp. 561–566, Nov. 2004, https://doi.org/10.5194/npg-11-561-2004.
30. L. Hudgins, C. A. Friehe, and M. E. Mayer, "Wavelet transforms and atmopsheric turbulence," *Phys Rev Lett*, vol. 71, no. 20, pp. 3279–3282, Nov. 1993, https://doi.org/10.1103/PhysRevLett.71.3279.
31. W. Soon, K. Dutta, D. R. Legates, V. Velasco, and W. Zhang, "Variation in surface air temperature of China during the 20th century," *J Atmos Sol Terr Phys*, vol. 73, no. 16, pp. 2331–2344, Oct. 2011, https://doi.org/10.1016/j.jastp.2011.07.007.
32. V. M. Velasco Herrera, W. Soon, G. Velasco Herrera, R. Traversi, and K. Horiuchi, "Generalization of the cross-wavelet function," *New Astronomy*, vol. 56, pp. 86–93, Oct. 2017, https://doi.org/10.1016/j.newast.2017.04.012.
33. P. C. Liu, "Wavelet Spectrum Analysis and Ocean Wind Waves," 1994, pp. 151–166.
34. V. Nourani, M. T. Alami, and F. D. Vousoughi, "Hybrid of SOM-Clustering Method and Wavelet-ANFIS Approach to Model and Infill Missing Groundwater Level Data," *J Hydrol Eng*, vol. 21, no. 9, Sep. 2016, https://doi.org/10.1061/(ASCE)HE.1943-5584.0001398.
35. N. Ullah *et al.*, "An Intelligent Framework for Fault Diagnosis of Centrifugal Pump Leveraging Wavelet Coherence Analysis and Deep Learning," *Sensors*, vol. 23, no. 21, p. 8850, Oct. 2023, https://doi.org/10.3390/s23218850.
36. I. Akoum, M. Graham, J. Kivihaho, J. Nikkinen, and M. Omran, "Co-movement of oil and stock prices in the GCC region: A wavelet analysis," *The Quarterly Review of Economics and Finance*, vol. 52, no. 4, pp. 385–394, Nov. 2012, https://doi.org/10.1016/j.qref.2012.07.005.
37. A. Fattouh, "An Emotional Model based on Wavelet Coherence Analysis of EEG Recordings," 2016.

SUPPLEMENTARY MATERIAL

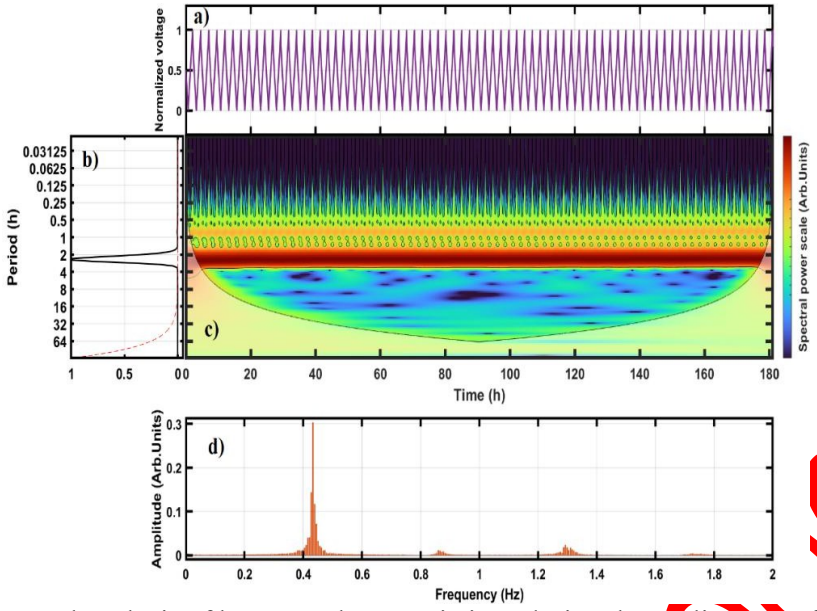

Figure S1. Spectral analysis of battery voltage variations during the cycling test of the SXC-2 cell: (a) Time series of battery voltage; (b) Global wavelet spectrum; (c) CWT power spectrum; and (d) Fourier spectrum analysis. The test was conducted by IER-UNAM

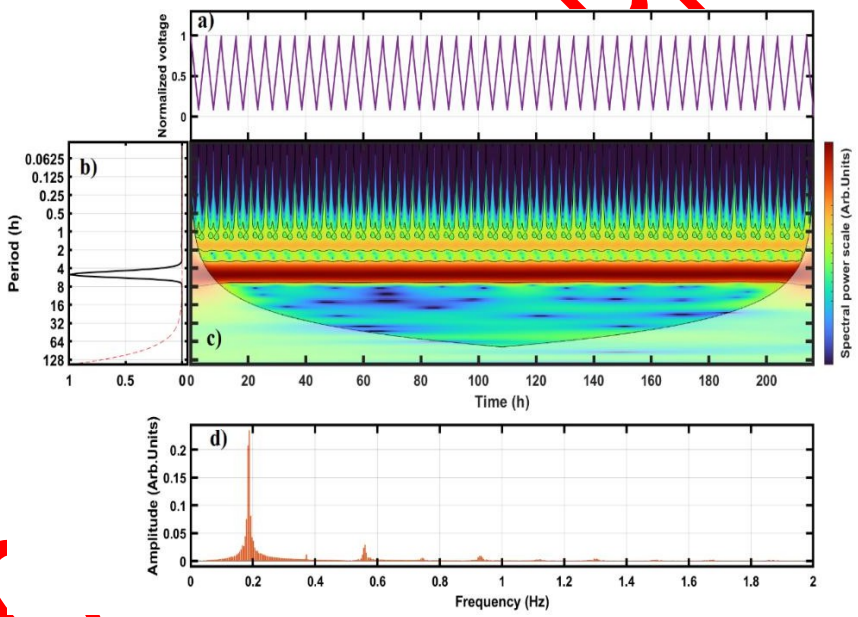

Figure S2. Spectral analysis of battery voltage variations during the cycling test of the SXC-3 cell: (a) Time series of battery voltage; (b) Global wavelet spectrum; (c) CWT power spectrum; and (d) Fourier spectrum analysis. The test was conducted by IER-UNAM

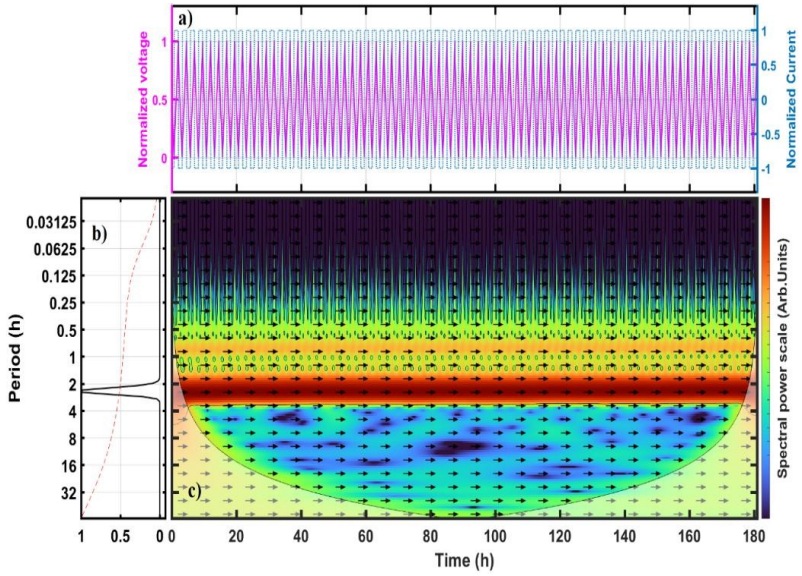

Figure S3. Cross-wavelet analysis of battery voltage and current variations during the cycling test of the SXC-2 cell: (a) Time series of normalized battery voltage (magenta) and normalized current (blue); (b) Global wavelet spectrum; and (c) XWT power spectrum. The test was conducted by IER-UNAM

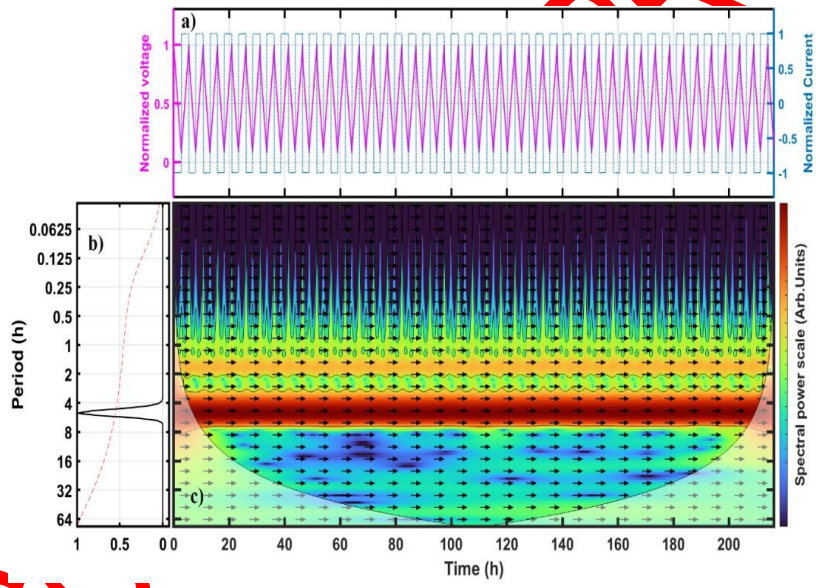

Figure S4. Cross-wavelet analysis of battery voltage and current variations during the cycling test of the SXC-3 cell: (a) Time series of normalized battery voltage (magenta) and normalized current (blue); (b) Global wavelet spectrum; and (c) XWT power spectrum. The test was conducted by IER-UNAM

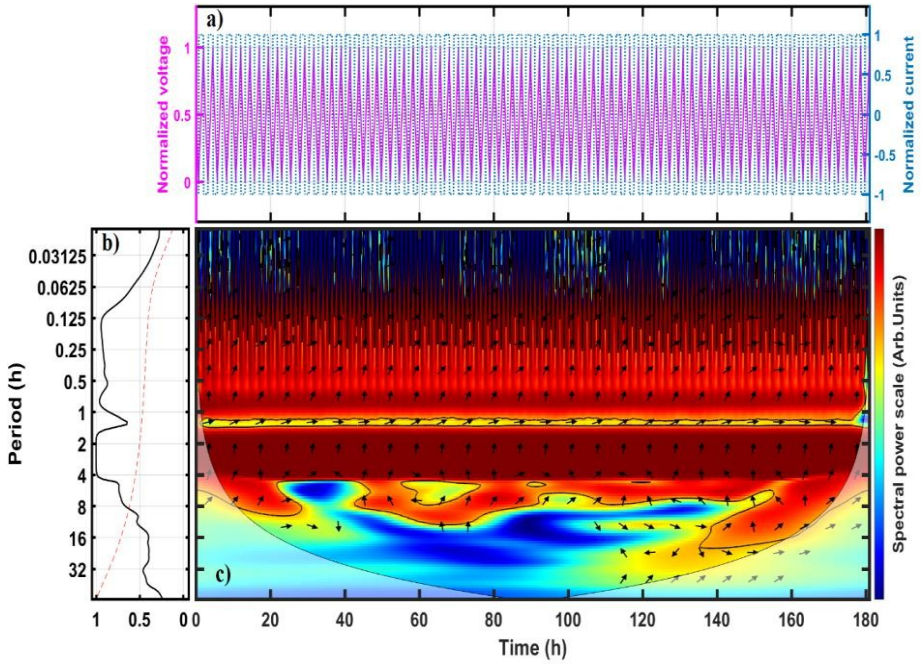

Figure S5. Wavelet coherence analysis of battery voltage and current variations during the cycling test of the SXC-2 cell: (a) Time series of normalized battery voltage (magenta) and normalized current (blue); (b) Global wavelet spectrum; and (c) WTC power spectrum. The test was conducted by IER-UNAM

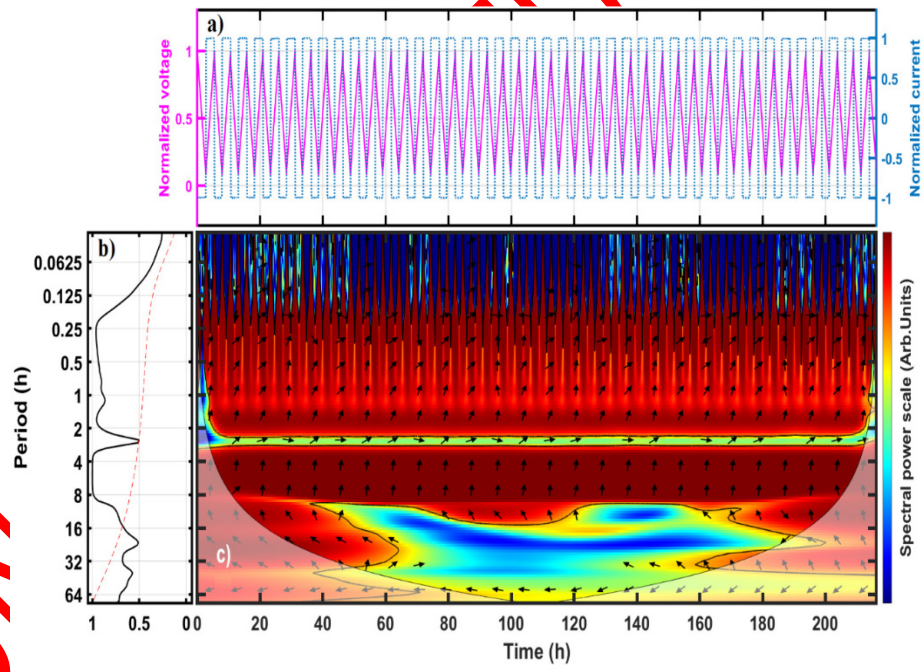

Figure S6. Wavelet coherence analysis of battery voltage and current variations during the cycling test of the SXC-3 cell: (a) Time series of normalized battery voltage (magenta) and normalized current (blue); (b) Global wavelet spectrum; and (c) WTC power spectrum. The test was conducted by IER-UNAM